Mechanistic Investigation of Rh(I)-Catalysed Asymmetric Suzuki-Miyaura Coupling with Racemic Allyl Halides

Lucy van Dijk,[a]† Ruchuta Ardkhean,[a,b]† Mireia Sidera,[a,c]† Sedef Karabiyikoglu,[a] Özlem Sari,[a,d] Timothy D. W. Claridge,[a]* Guy C. Lloyd-Jones,[f]* Robert S. Paton,[a,e]* and Stephen P. Fletcher[a]*

[a] Department of Chemistry, Chemistry Research Laboratory, University of Oxford, 12 Mansfield Road, Oxford, OX1 3TA, UK.

[b] Faculty of Medicine and Public Health, HRH Princess Chulabhorn College of Medical Science, Chulabhorn Royal Academy, Bangkok, Thailand.

[c] Vertex Pharmaceuticals (Europe) Ltd, 86-88 Jubilee Avenue, Milton Park, OX14 4RW, UK.

[d] Department of Chemistry, Middle East Technical University, 06800 Ankara, Turkey; Department of Chemistry, Kirsehir Ahi Evran University, 40100, Kirsehir, Turkey.

[e] Department of Chemistry, Colorado State University, Fort Collins, CO 80523, USA

[f] EaStChem, University of Edinburgh, Joseph Black Building, David Brewster Road, Edinburgh, EH9 3FJ, United Kingdom.

† L.v.D, R.A and M.S. contributed equally to this work.

Abstract

Understanding how catalytic asymmetric reactions with racemic starting materials can operate would enable new enantioselective cross coupling reactions giving chiral products. Here we propose a catalytic cycle for the highly enantioselective Rh(I)-catalysed Suzuki-Miyaura coupling of boronic acids and racemic allyl halides. Natural abundance ^{13}C kinetic isotope effects provide quantitative information about the transition state structures of two key elementary steps in the catalytic cycle – transmetalation and oxidative addition. Experiments using configurationally stable, deuterium labelled substrates reveal oxidative addition can happen *via syn*- or *anti*-pathways which control diastereoselectivity. DFT calculations attribute the extremely high enantioselectivity to reductive elimination from a common Rh complex formed from both allyl halide enantiomers. Our conclusions are supported by analysis of the reaction kinetics. These insights into the sequence of bond-forming steps and their transition state structures will contribute to understanding asymmetric Rh-allyl chemistry and enable the discovery and application of asymmetric reactions with racemic substrates.

Introduction

Suzuki-Miyaura cross-coupling is used extensively for C(sp^2)–C(sp^2) bond formation (Fig. 1a). One reason for the broad adaptation of this method is the wide range of organoboron reagents that are readily available and easy to handle, providing advantages over other organometallic reagents.[1] Since the first report in 1979, tremendous effort

has been directed towards further development, leading to Suzuki's receipt of the 2010 Nobel Prize in Chemistry alongside Heck and Negishi.[2]

The development of asymmetric cross-coupling transformations with organoboron reagents is an area of active investigation. Reported strategies include starting from single enantiomer alkylboronates, enantiopure electrophiles, and desymmetrisations.[3] Boronic acids and derivatives have been employed in enantioselective allylic arylations mostly catalysed by Rh,[4, 5] Cu,[6] Pd[7] and Ni.[8] Some stereospecific allylic arylations have also been developed using Pd[9] and Cu.[10]

We have developed a highly enantioselective Suzuki-type coupling between arylboronic acids and racemic cyclic allyl halides catalysed by Rh-bisphosphine complexes (Fig. 1b).[11] We have demonstrated the use of vinyl and (hetero)arylboronic acids in combination with racemic (hetero)cyclic electrophiles.[12] The versatility of the method was highlighted by synthesis of the natural product (+)-isoananbasine,[12] and anticancer agent niraparib (Fig. 1b).[13] However, this transformation is currently limited to electrophiles that, after cleavage of the carbon–halogen bond, are achiral about the allyl unit.[13, 14]

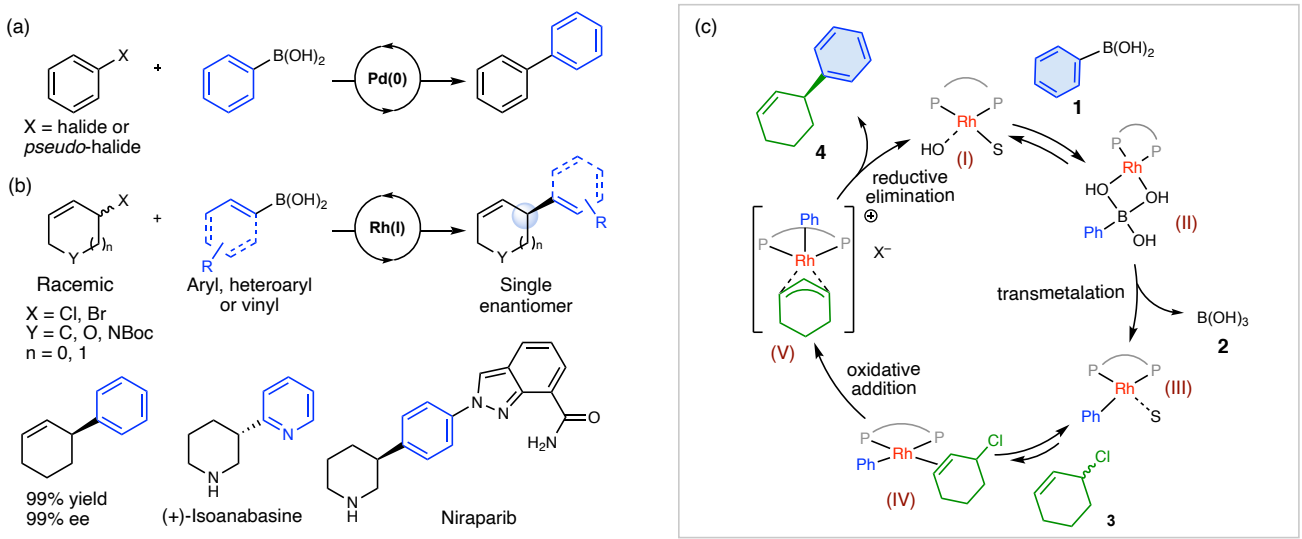

Figure 1. Suzuki-Miyuara cross coupling (a) Classical Suzuki-Miyuara coupling. (b) The enantioselective Rh-catalysed Suzuki-Miyaura coupling to form C(*sp*^{3})-C(*sp*^{2}) bonds and selected compounds which can be synthesised using this method. (c) A simplified catalytic cycle showing the proposed mechanism in this work with key steps including transmetalation, oxidative addition and reductive elimination.

Detailed mechanistic studies on Rh-catalysed asymmetric additions are scarce. Hayashi and co-workers reported a key study on additions of arylboronic acids to cyclic α,β-unsaturated ketones.[15] For that transformation, after transmetalation, 2-cyclohexenone inserts into the Rh-aryl bond to form an oxa-π-allyl Rh species which hydrolyses to release the product. A subsequent kinetic study revealed that transmetalation from boron to Rh was the rate-

determining step.[16]

Asymmetric allylic addition reactions with racemic electrophiles may occur *via* several distinct mechanistic pathways. Dynamic kinetic asymmetric transformations (DYKATs) catalysed by Pd using stabilised nucleophiles occur *via* a well-understood mechanism; both enantiomers of the starting material are converted to a common pseudo-prochiral intermediate, and a subsequent outer-sphere addition of the nucleophile creates the new stereogenic centre.[17] A similar DYKAT mechanism may be operative here where oxidative addition of both enantiomers of the substrate results in a Rh-allyl species. Transmetalation of that species would be followed by an inner-sphere nucleophilic attack to give the arylated product.[18]

Cu-catalysed asymmetric addition of alkylzirconium reagents to racemic allylic substrates,[19] in contrast to Pd-catalysed mechanisms, involves dynamic kinetic resolution facilitated by a Cu-halide-ligand complex.[20] The complex acts to interconvert enantiomers of the allyl chloride, as well as catalyse addition, and one enantiomer reacts more readily to give an enantioenriched product. The Rh-catalysed arylation here could operate *via* a related mechanism, involving facile interconversion of substrate enantiomers followed by a stereospecific addition step.

Rh-catalysed hydroarlyation and Rh-catalysed processes involving diene electrophiles are known.[21-23] A mechanism could be operative here where elimination of the allyl halide forms a diene intermediate which then undergoes hydroarylation with a Rh-aryl species. Other plausible mechanisms include various radical processes,[24, 25] and direct enantioconvergent processes where the two starting enantiomers react *via* different mechanistic pathways to give the same enantiomer of the product.[26]

In order to further understand the limitations and potential of Rh-catalysed asymmetric additions and of catalytic processes involving racemic substrates, we set out to design a series of experimental and computational experiments to reveal the mechanisms involved in this transformation. Here, we discuss our experimental and computational studies that rule out the mechanistic scenarios outlined above, and instead are fully consistent with the proposal shown in Fig. 1c. The available evidence is congruent with the scenario in which a monomeric active catalytic species (**I**) reacts with the arylboronic acid (**1**) forming a Rh-aryl intermediate (**II**). Irreversible oxidative addition with both allyl chloride enantiomers yields a common η^3 complex (**V**), although one enantiomer of **3** reacts faster than the other. The subsequent reductive elimination step is enantiodetermining and sets the configuration of the product, as dictated by the absolute stereochemistry of the ligand.

Results

Preliminary NMR Spectroscopic and Mechanistic Experiments

NMR spectroscopy was used to examine the reaction between $[Rh(cod)(OH)]_2$ and (*S*)-Xylyl-P-Phos ((*S*)-**L1**) in THF-d_8. By comparing our data with literature reports,[15] we identified the formation of pre-catalytic species $[Rh(\mathbf{L1})(OH)]_2$ and the mixed $[Rh_2(cod)(\mathbf{L1})(OH)_2]$ dimer. Rh-ligand dimer $[Rh(\mathbf{L1})(OH)]_2$ undergoes rapid reaction with phenylboronic acid to give a Rh-aryl species. In contrast, when allyl chloride **3** was added to $[Rh(\mathbf{L1})(OH)]_2$, no reaction was observed even upon heating. These observations are not consistent with mechanisms initiated by the allylic electrophile first reacting with a metal-complex.[18]

Strikingly, formation of the pre-catalyst $[Rh(\mathbf{L1})(OH)]_2$ did not give a single clean species and was often accompanied by varying amounts of other species featuring ^{31}P singlet peaks at 25.7, 24.2 and –14.7 ppm, which we attribute to mono- and di-oxidised forms of ligand. Attempts to further characterise this reaction using *in situ* NMR spectroscopy were hindered by formation of complex mixtures of phosphorous containing species, which was not overcome by using alternative Rh complexes.

In related Cu-catalysed transformations, we observed the interconversion of substrate enantiomers.[20] To examine if a similar process was occurring here, we used ^1H NMR exchange spectroscopy. However, under the reaction conditions, no exchange between vinylic and allylic protons in **3** was observed on the NMR timescale suggesting that the allyl chloride enantiomers don't interconvert *via* an S_N2' mechanism or do so at a much slower rate than ^1H NMR relaxation. Therefore, a dynamic kinetic resolution mechanism appears unlikely. This does not preclude racemisation occurring during these reactions - it simply suggests that this is not a fundamental requirement of the reaction. A limitation of this experiment is that interconversion *via* S_N2 mechanisms cannot be detected.

To better understand the active catalytic species, we probed for nonlinear effects by measuring product (**4**) ee as a function of ligand (**L1**) ee.[27] A linear correlation between the enantiopurity of **L1** and **4** was observed, providing no evidence for the involvement of high-order aggregates of the catalyst, consistent with an active catalytic species monomeric in Rh and **L1** (supplementary Fig. 1).

To test if the reaction could occur *via* the formation of an intermediate diene species, we used cyclohexa-1,3-diene in place of **3** but observed no arylated product. A reaction using d_5-phenylboronic acid showed the deuterium labels remained on the phenyl ring, ruling out mechanisms involving insertion of the Rh catalyst into C-H bonds of the aromatic ring.[22]

Transmetalation

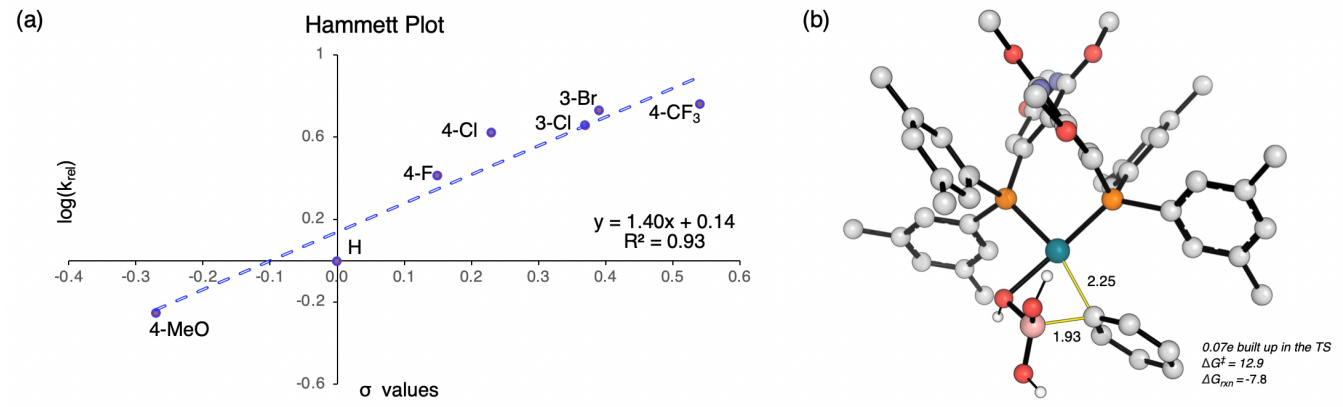

Figure 2. Examining the transmetalation step using experimental and computational techniques (a) A Hammett plot constructed from results of competition experiments between various meta- and para-substituted arylboronic acids. σ values = Hammett substituent constants, k_{rel} = relative rate (b) The DFT-computed transmetalation transition structure (ωB97X-D/6-31G(d), LANL2DZ(f)). TS = transition structure, $\Delta G^{\ddagger}$ = activation energy, ΔG_{rxn} = change in Gibbs Free Energy.

To probe the transmetalation step, we carried out a series of competition experiments using different arylboronic acids. There is a strong positive correlation between the ratio of products obtained and the Hammett substituent constants (σ values) of the arylboronic acids (Fig. 2).[28, 29] This indicates transmetalation is faster with electron withdrawing substituents on the arylboronic acid, allowing electron deficient aryl species to preferentially and irreversibly enter the catalytic cycle, leading to formation of one product in excess. This preferential transmetalation could be due to increased Lewis acidity of the boron favouring formation of the boronate, and/or enhanced ability of electron poor substrates to stabilise partial negative charge during transmetalation.[30,31] We surmise that a key role of the base in these reactions is to aid in the formation of boronate species. Consistent with our experimental observations, the accumulation of negative charge in the aromatic ring was observed in the DFT-computed transition structure (TS). Relative to the pre-transmetalation intermediate with a Rh-O-B linkage,[31,32] this elementary step is exergonic by 7.8 kcal/mol, consistent with irreversibility.

Natural abundance ^{13}C kinetic isotopic effects

We next focused our attention on the ensuing reaction between aryl-Rh species (**III**) and allyl chloride **3**, for which various possible mechanisms could be envisaged. To gain more understanding we sought to determine natural abundance $^{12}C/^{13}C$ ratios using the method developed by Singleton.[33,34] This approach has been employed with great success to measure competitive intermolecular ^{13}C kinetic isotope effects (KIE) in mechanistic studies of catalytic reactions.[35-43] This commonly relies on running the reaction to high conversion, and examining the $^{12}C/^{13}C$

ratio in recovered starting material. However, in the asymmetric addition to **3**, the isolation of small amounts of starting material at high conversions isn't possible as **3** is too sensitive to be reliably purified and may be configurationally labile during reaction or work-up conditions.[20] It is also plausible that the two enantiomers of **3** could undergo conversion at different rates, confounding analysis of KIE by examining the starting material. We therefore chose to determine $^{12}C/^{13}C$ ratios generated in product **4** when the reaction is quenched at low conversion and quantify the depletion of ^{13}C by quantitative ^{13}C NMR spectroscopy.

We performed the reactions on a 7.0 mmol scale as a relatively large amount of product is required for quantitative ^{13}C NMR spectroscopy and the reaction must be stopped at low conversion to ensure the product is enriched in the faster reacting isotope. However, using optimised conditions at this scale at 60 °C, the reaction was much faster than anticipated; when the reaction was quenched after 2 min, the conversion was already 60%. Suitable results could be obtained by stirring the reaction at 40 °C and quenching after 20 seconds. We repeated the process three times under these conditions, with experiments giving 10, 11 and 17% conversion (Fig. 3a). For the quantitative ^{13}C spectroscopy, we took C5 as the reference carbon. Although ^{13}C KIE are intrinsically small (ranging from 0.98–1.10),[44] after running these experiments in triplicate we observed appreciable KIE at positions C1, C3 and C7 (Fig. 4a).

For multi-step catalytic mechanisms, any observed isotope effects are the result of isotopic fractionation occurring at or before the first irreversible step that involves that reaction component.[45] Experimentally, we measured the largest KIE at C7 (1.027 ±0.006) and C3 (1.024 ±0.003), and a smaller, but still significant, KIE was obtained at C1 (1.010 ±0.005). As the transmetalation step is irreversible, ^{12}C fractionation at the aryl ipso-carbon (C7) of the product is most likely the result of a KIE in this elementary step.

To interpret the enrichment observed at C1 and C3, we calculated $^{12}C/^{13}C$ KIE that would result from various addition mechanisms (S_N2, S_N2'and reversible *anti*-oxidative addition). The KIE values were calculated according to transition state theory applying the Bigeleisen–Mayer equation using scaled vibrational frequencies.[46,47] The calculated results for the most likely mechanism, as judged by comparing experimental and theoretical results, are shown in Fig. 3b-d.

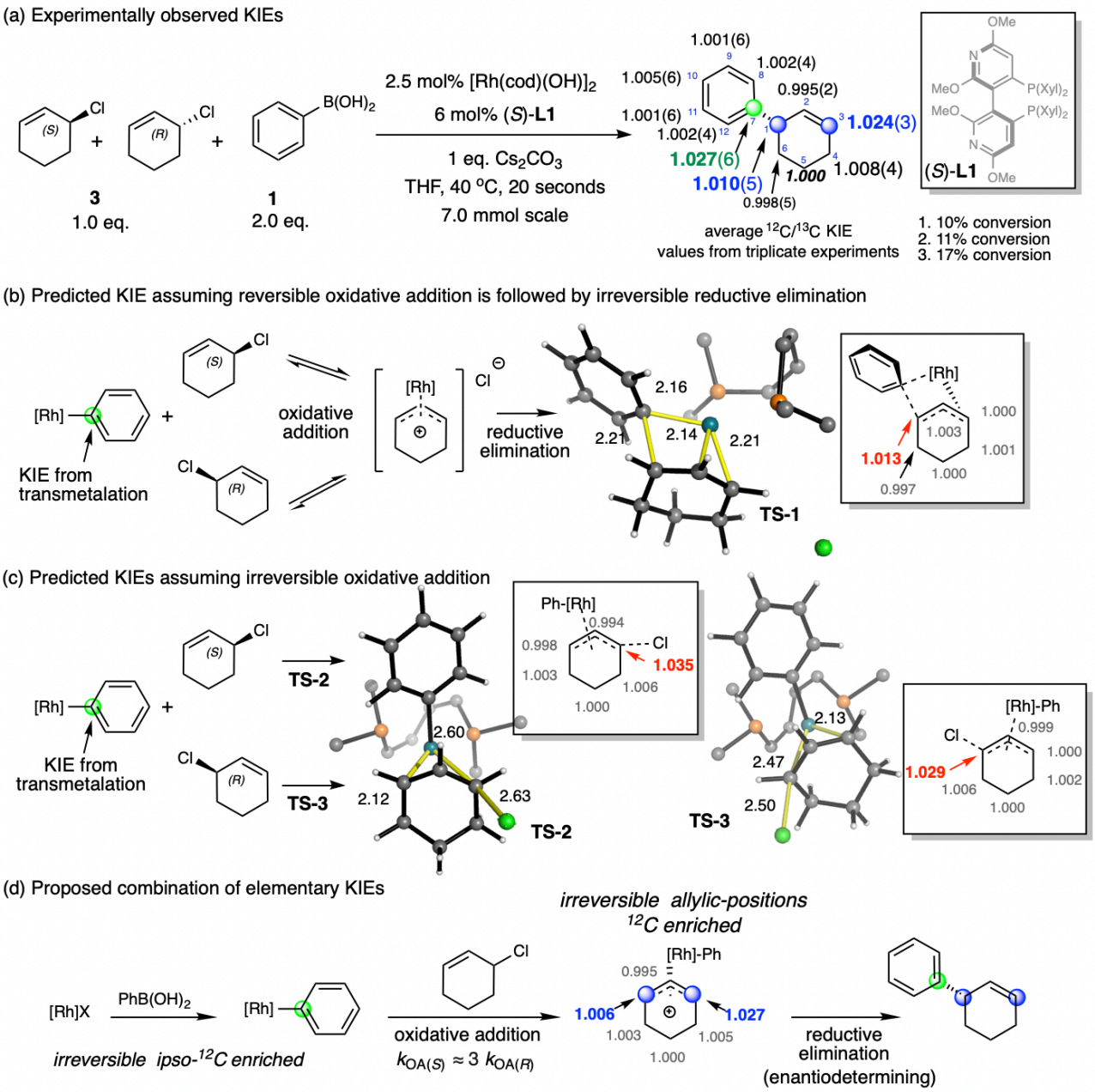

Figure 3. Examining the ^{13}C Kinetic Isotope Effect (a) ^{13}C KIE experimental results, standard errors in parenthesis. (b) Calculated ^{13}C KIE of stepwise mechanism with reversible *anti*-oxidative addition followed by irreversible reductive elimination. (c) Calculated ^{13}C KIE of stepwise mechanism with irreversible *anti*-oxidative addition. (d) Proposed combination of elementary KIE. A ratio of ~3.3:1 for oxidative addition of the *S* over the *R* enantiomer of the starting allyl chloride gives the observed level of ^{12}C enrichment. Computed TSs are shown with cropped ligands for clarity; selected distances are shown in Å.

In our proposed DYKAT mechanism with *anti*- oxidative addition followed by reductive elimination, there are two plausible scenarios; one where oxidative addition is reversible and reductive elimination is the first irreversible step involving **3** (Fig. 3b), and another where oxidative addition is the first irreversible step in which **3** is involved (Fig. 3c). In the first scenario (Fig. 3b), the calculated KIE of C1 is 1.013 but there is no significant KIE at C3. The

calculated KIE of only two carbons are within the experimental errors of the measured KIE. In the second scenario where oxidative addition is irreversible, the calculated KIE starting with (*S*)-**3** gave a value of 1.035 on C3, whereas with (*R*)-**3** gave KIE of 1.029 on C1 (Fig. 3c). If both enantiomers of **3** undergo an irreversible oxidative addition, albeit at different rates, the observed KIE from product analysis will be a weighted average from both starting enantiomers. From our calculations, a 3.3:1 ratio of (*S*)- to (*R*)-**3** undergoing oxidative addition accounts quantitatively for the experimentally observed KIE on all six carbons of the allyl unit (Fig. 3d).

These experiments are inconsistent with other possible mechanisms for the Rh-catalysed process. Overall, the ^{13}C KIE support a mechanism where the first step in the catalytic cycle is an irreversible transmetalation, followed by an irreversible *anti*-oxidative addition where the enantiomers of **3** react at different rates.

DFT calculations

DFT calculations[48] were performed using the ωB97X-D functional.[49] In geometry optimisations, LANL2DZ(f) (orbital exponent of 1.35) effective core potential (ECP)/valence double-ζ basis set was used for Rh and the split-valence 6-31G(d) basis set was used for other atoms. Single point energy corrections were obtained with an implicit description of the reaction medium by SMD solvent model at the ωB97X-D/6-311+G(d,p) level of theory with the LANL2TZ(f) ECP/valence triple-ζ basis set for Rh. The Gibbs energy profile for transmetalation, oxidative addition and reductive elimination steps are illustrated in Fig. 4. Other possible mechanisms were also calculated but found to have higher reaction barriers (Supplementary Fig. 5).

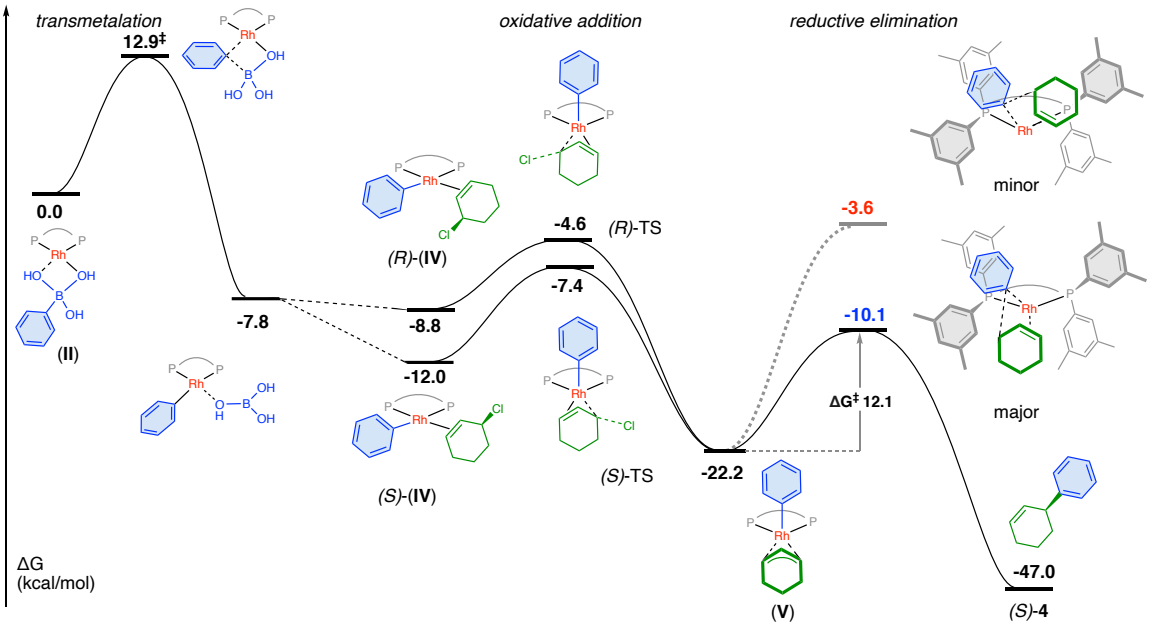

Figure 4. A condensed Gibbs energy profile showing transmetalation, oxidative addition and reductive elimination. SMD(THF)-ωB97X-D/6-311+G(d,p), LANL2TZ(f) // ωB97X-D/6-31G(d), LANL2DZ(f). ΔG = change in Gibbs Free Energy, $\Delta G^{\ddagger}$ = activation energy.

Calculations suggest that the key process for enabling the use of racemic **3** in this DYKAT is oxidative addition to give a common η-3 intermediate (**V**) where the stereochemical information of **3** is lost. The energy barrier of oxidative addition for (*R*)-**3** is calculated to be higher than (*S*)-**3**, in qualitative agreement with natural abundance ^{13}C KIE experiments. Subsequently, the intermediate undergoes reductive elimination wherein the stereochemistry of the product is set due the spatial constraints the C_2-symmetric ligand imposes on the allyl unit and the phenyl group. From these calculations we deduce that reductive elimination is enantiodetermining, as the new stereogenic center is predicted to form irreversibly in this step.[50] The large calculated difference in energy between the reductive elimination TSs ($\Delta\Delta E^{\ddagger}$ = 5.5 kcal/mol, $\Delta\Delta G^{\ddagger}$ = 7.2 kcal/mol) is consistent with both the sense and very high levels of enantioselectivity observed experimentally for the formation of (*S*)-**4** in >99% ee. Transmetalation and oxidative addition steps are both predicted to take place irreversibly. The consequence of an irreversible oxidative addition is that the diastereoselectivity is determined in this step.

Reaction kinetics

The kinetics of the Rh-catalysed reaction of (4-fluoro-3-methylphenyl)boronic acid (**1a**) with cyclohexenyl chloride **3**, using ligand (*S*)-**L1**, were explored under a range of conditions that ensured that solution-phase reactions, not mass-transfer processes, were rate-limiting. Whilst considerable variation in rates were found between reactions conducted with various commercial sources of (*S*)-**L1** and $[Rh(cod)(OH)]_2$, kinetic data were found to be reproducible within batches, and all runs were conducted in triplicate. Temporal concentrations were determined by ^{19}F NMR analysis of a series of eight samples taken at 90-second intervals from the reaction mixtures, over a period of 720 seconds, using 4,4'-difluoro-1,1'-biphenyl as an internal standard for integration. Systematic variation of the initial concentrations of the cyclohexenyl chloride **3** (0.1, 0.05, and 0.025 M), total Rh (0.0025, 0.005, and 0.0075 M), and the (4-fluoro-3-methylphenyl)boronic acid **1a** (0.1, 0.3, and 0.4 M), afforded product evolution profiles that suggested progressive inhibition.

Equation 1

$$\frac{d[\mathbf{4a}]}{dt} \approx \frac{[Rh]_{TOT}}{a + \frac{b}{[\mathbf{3}]} + \frac{c\,[\mathbf{2}]}{[\mathbf{1a}]}}$$

a = 9.0±2.6 s
b = 2.3±0.5 ×10^{-1} M s
c = 4.2±0.3 ×10^{2} s

Experiments with exogenous boric acid (**2**) identified inhibition arising from the accumulating $Cs[B(OH)_4]$ co-product, that is assumed to compete with the arylboronate for coordination to Rh-OH complex (**I**). All eight datasets could be satisfactorily simulated using a kinetic model based on all of the key mechanistic features evaluated in a pseudo steady-state rate equation (Equation 1) with five concentration terms ($[Rh]_{TOT}$; **4a** (arylation product); **2**

(boric acid); **1a** (boronic acid); and **3** (cyclohexenyl chloride) and three simplified empirical constants, *a*, *b*, and *c* (Supplementary Fig. 2 and 3). The analysis indicates that the reactions proceed with first order dependence on $[Rh]_{TOT}$, and apparent orders in cyclohexenyl chloride **3** and arylboronate **1a** that evolve between limits of pseudo zero-order to first-order as the reactions proceed, with no simple relationships dominant for either component.

Arylation with Heterocyclic and Other Allyl Chlorides

We also calculated the energy profile for the pyranyl substrate **5** and found that the barrier to oxidative addition is much lower than that of **3** (Supplementary Fig. 6). A competition experiment between allyl chlorides **3** and **5** was performed (Fig. 5a). After 1 hour, the product ratio was 20:1 in favour of product **6**, indicating that oxidative addition is faster for **5** which is qualitatively in agreement with the results of our DFT calculations.

Both ^{13}C KIE experiments and DFT calculations suggests that there are differences in the rate of oxidative addition of the enantiomers of (±)-**3**. Based on this hypothesis, an increase in ee of **3** over the course of the reaction would be anticipated. Despite several attempts, the ee of **3** could not be reliably measured and enantiopure **3** likely cannot be obtained due to its high reactivity,[20] precluding us from directly probing the relative rate of oxidative addition of the enantiomers of **3**. However, this could be probed using piperidinyl allyl chloride **7** which was found to be configurationally stable.[51]

We monitored the ee of **7** under the conditions used in the ^{13}C KIE measurements and found that the ee of **7** increases from 0 to 94% ee over 1 hour (Fig. 5b), supporting the idea that the rate of oxidative addition differs for the two enantiomers of the substrate. This also supports our earlier conclusion that fast interconversion of substrate enantiomers is not required for this asymmetric reaction.

Interestingly, under alternative conditions, previously optimised for **7**, using (*S*)-**L2**, enantioenrichment of **7** was not observed (Fig. 5d). This observation was unchanged at a 30 ºC, and so the resolution of starting materials is likely a ligand effect. These ligands impose different steric environments on the oxidative addition TSs therefore leading to different relative energies between the oxidative addition TSs of the two enantiomers of the allyl chloride. Under the conditions shown in Fig. 5d, both enantiomers of **7** may react at comparable rates due to reduced steric constraints in the oxidative addition TSs.

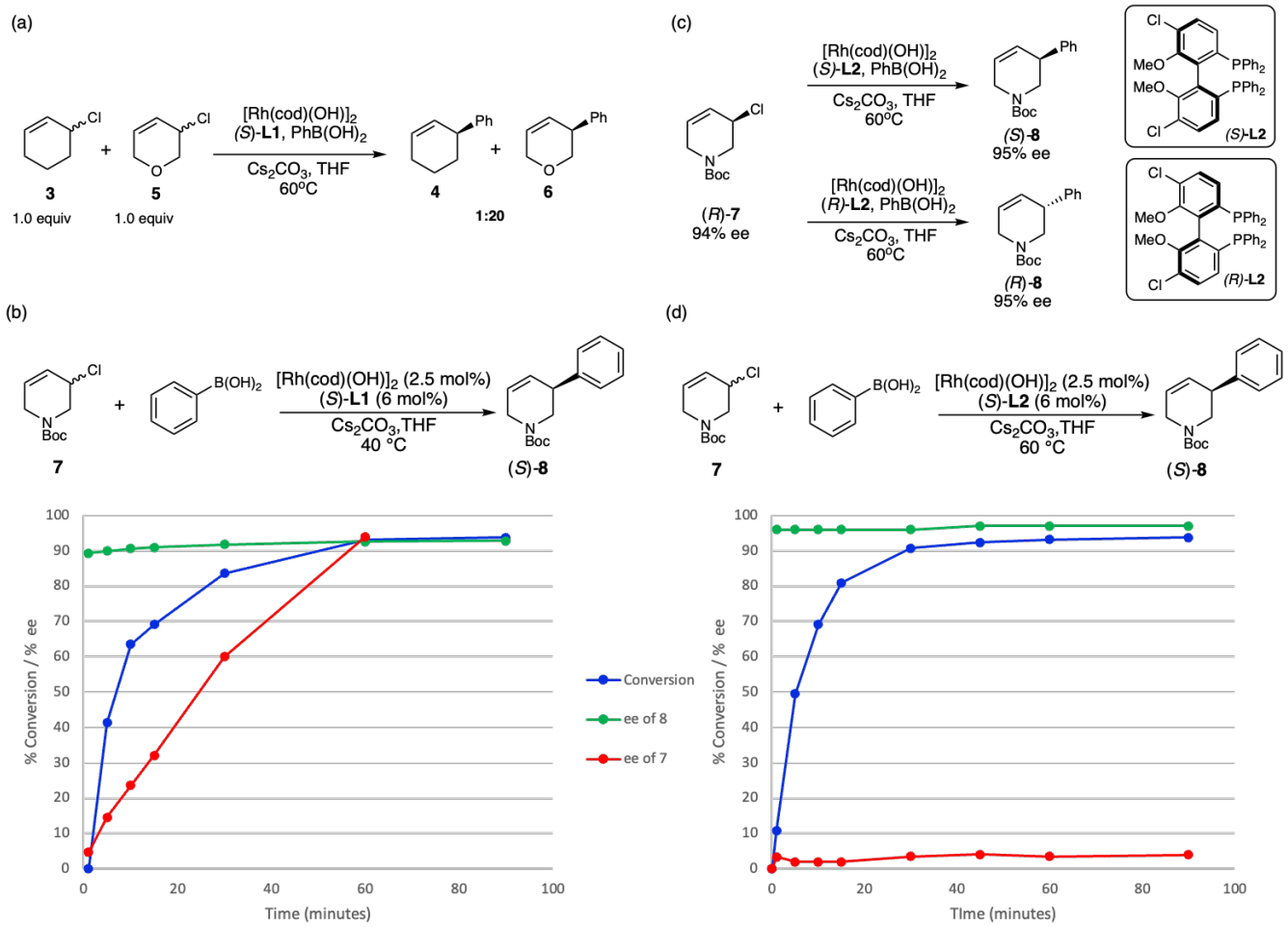

Figure 5. Asymmetric allylic arylation with heterocyclic allyl chlorides (a) Competition experiment with allyl chlorides (±)-**3** and (±)-**5**. (2.5 mol % $[Rh(cod)(OH)]_2$, 6 mol % **L1**, 1 equiv. of $PhB(OH)_2$). Complete conversion of $PhB(OH)_2$ to arylated product observed. (b) Measuring the ee over the course of the reaction with allyl chloride **7** using **L1**. (c) Arylation of enantioenriched (+)-**7** with both enantiomers of **L2**. (2.5 mol % $[Rh(cod)(OH)]_2$, 6 mol % **L2**, 2 equiv. of $PhB(OH)_2$) >85% conversion of **7** to arylated product observed. (d) Measuring the ee over the course of the reaction with allyl chloride **7** using **L2**.

In both of these experiments, we observed that the ee of **8** is constant as a function of time, supporting the idea that reductive elimination is the stereodetermining step.

We were able to access enantioenriched (*R*)-**7**,[51] and subjected (*R*)-**7** (94% ee) to reaction conditions with each enantiomer of **L2** (Fig. 5c). With (*S*)-**L2**, we obtained (*S*)-**8** (95% ee), whereas with (*R*)-**L2**, the other enantiomer of the product ((*R*)-**8,** –95% ee) was obtained. Therefore, the absolute stereochemistry of the product is determined by the stereochemistry of the ligand and isn't affected by the stereochemistry of the allyl chloride. Interestingly, with

(*R*)-**L2**, the reaction was considerably slower, and we observed deterioration of the ee of (*R*)-**7** (94% to 82% ee over 6 hours), suggesting that racemisation may occur slowly but it isn't essential for product formation.

Isotopically labelled **7**-*d* was synthesised with a deuterium atom at the vinylic position.[51] Under the conditions shown in Fig. 7a, addition to (±)-**7**-C3-*d* gave a 1:1 ratio of products with deuterium at C3 and C5. Due to the ^{2}H-label at the vinylic position in each enantiomer of starting material, the two enantiomers can no longer form a common intermediate after oxidative addition. One enantiomer reacts to give one intermediate which, after reductive elimination, leads to one pseudo-regioisomer of the product and the other reacts to give the alternative pseudo-regioisomer.

Therefore, if enantioenriched ^{2}H-labelled **7** is used the products should have an excess of the deuterium label at one position (allylic or vinylic) depending on the stereochemistry of the ligand used. After subjecting (*R*)-**7**-C3-*d* (94% ee) to optimised reaction conditions with (*S*)-**L2**, the majority of deuterium remained at C3 in product (*S*)-**8**, whereas with (*R*)-**L2**, the majority of deuterium was found at the allylic position of (*R*)-**7** (Fig. 6b).

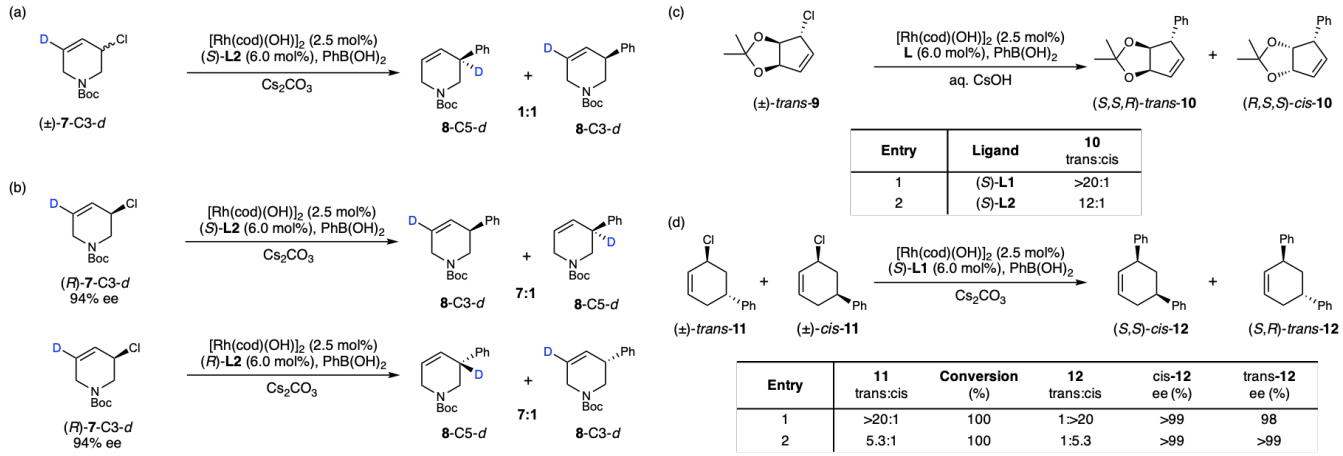

Figure 6. Asymmetric allylic arylation with deuterium labelled allyl chlorides and diastereomeric allyl chlorides (a) Arylation of (±)-*d*-**7**. (b) Arylation of (*R*)-*d*-**7** with both enantiomers of **L2**. (c) Arylation of bicyclic substrate **9** showing evidence for *syn*-oxidative addition. (d) Arylation of diastereomeric 5-phenyl substituted starting materials showing evidence for *anti*-oxidative addition. All reactions were performed in THF at 60 °C.

Deuterium-labeled substrates can be used to assess the stereochemical outcome of the individual steps of allylic substitution reactions.[52-55] According to our proposed mechanism of *anti*-oxidative addition, we expected ((*R*)-**7**-C3-*d*) to give the opposite results obtained in terms of observed pseudo-regioisomer preference with each enantiomer of the ligand. Our experimental results surprisingly indicate that with **7**, *syn*-oxidative addition is the major pathway. In each case, there is a small percentage of deuterium scrambling (7:1 ratio) which we attribute to a 7:1 ratio of *syn* and *anti*-oxidative addition steps occurring. At this stage we cannot rule out that the scrambling

is due to slow racemisation of **7** over the course of the reaction, or alternatively isomerisation after oxidative addition *via* nucleophilic displacement with Rh(I) species in analogy to mechanistic pathways observed in Pd(0)-catalysis.[56]

Recently, we discovered that the related Rh-catalysed enantioselective additions to fused bicyclic substrates give stereochemical results consistent with *syn*-selective addition to racemic allyl chloride starting materials (Fig. 6c).[14] To further probe these experimental results, we compared the *syn*- and *anti*- transition states arising from oxidative addition to **9** using DFT calculations (see Fig. 7a for favoured *syn*-TS). The results show that steric clash between the substrates acetal bridge and ligand used is key to determining the facial selectivity of oxidative addition. It is important to note here that oxidative addition is the diastereodetermining step in this system, while reductive elimination remains in control of the absolute stereochemistry.

DFT calculations for model substrate **3** (Fig. 4 and 7) clearly indicate that in **3** *anti*- oxidative addition is favoured. We have also examined enantioselective additions to phenyl-substituted allyl chlorides,[11] where mixtures of the four stereoisomers of 3-chloro-5-phenylcyclohex-1-ene (**11**) gave overall enantioselective inversion to *cis*- and *trans*-**12** (Fig. 6d). These experiments, where we observe highly enantioselective overall inversion to form *cis*- and *trans*-**12**, are consistent with *anti*- oxidative addition with an aryl-Rh species, followed by inner-sphere attack of the aryl nucleophile, delivering the phenyl on the same side of the allyl ion as the Rh.

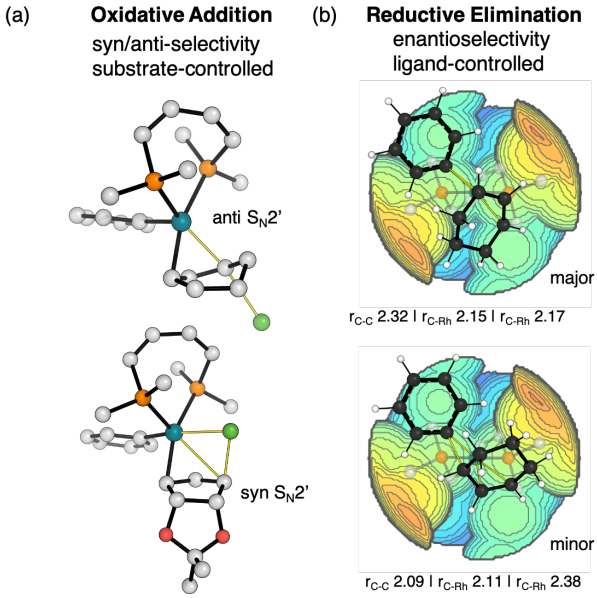

Figure 7. Simplified models showing the origins of diastereoselectivity and enantioselectivity in this Rh(I)-Catalysed Asymmetric Suzuki Miyaura Coupling (a) Favoured *anti*-oxidative addition TS for **3** and favoured *syn*-oxidative addition TS for **9**. (b) Reductive elimination TSs for **3**. Catalytic pocket images generated using: SambVca 2.1.[52]

Therefore, we have experimentally observed and computationally validated that Rh species can add to allyl halide substrates *via syn*- or *anti*-oxidative addition, depending on the steric accessibility of the substrate (Fig. 7a). The oxidative addition step dictates diastereoselectivity and is influenced by the substrate, while the overall sense of enantioselectivity is catalyst-controlled and set in the reductive elimination step. The high enantioselectivity observed experimentally is reflected in the large difference in energy between the reductive elimination transition states. This can be attributed to steric effects between the ligand and allyl fragment, which in turn give rise to substantial differences in key bond distances between the two competing TSs. An analysis of the catalytic pocket (Fig. 7b) emphasises the narrow groove provided by the ligand in which the reductive elimination must take place.[57] The minor TS structure has weaker coordination between alkene and Rh, and a much shorter forming C-C bond (i.e. a later TS) – compared to the favoured structure, which is consistent with the large energy difference between the two.

Conclusions

The asymmetric Suzuki-Miyaura coupling of arylboronic acids with racemic allylic halides catalysed by a Rh(I) complex gives highly enantioenriched arylated products. We have used a variety of techniques to elucidate a mechanistic proposal and the key mechanistic features of this proposal are fully consistent with detailed analysis of the reaction kinetics. Here the active catalytic species is monomeric in Rh and ligand and irreversible transmetalation between boron and Rh is the first step in the catalytic cycle. Experimentally observed natural abundance ^{13}C KIEs in combination with theoretical calculations were key to demonstrating that oxidative addition occurs in a ~3.3:1 ratio in favour of one enantiomer over the other. A common pseudo-symmetrical η^3 Rh-allyl complex is formed by irreversible oxidative addition of Rh-aryl intermediates to both enantiomers of the racemic substrates. Interestingly, oxidative addition can occur in a *syn*- or *anti*- fashion depending on the steric accessibility of the substrate. The symmetry of η^3 Rh-allyl complexes formed by oxidative addition was probed using configurationally stable, racemic and enantiomerically enriched, and deuterium labelled piperidinyl allyl chlorides along with racemic diastereomeric substituted allyl chlorides. These studies support the proposed promiscuity of the oxidative addition step and demonstrate that reductive elimination of common intermediates formed from both enantiomers give highly enantioenriched products where the diastereoselectivity is determined by oxidative addition and absolute stereochemistry of the product is dictated by the ligand.

We foresee that this study will contribute to the broader understanding of asymmetric Rh-allyl chemistry and will enable the discovery, exploitation and understanding of new asymmetric reactions with racemic substrates.

Methods

Instrumentation and materials

Procedures using oxygen and/or moisture-sensitive materials were performed with anhydrous solvents under an atmosphere of argon in flame-dried flasks, using standard Schlenk techniques. Dry THF and CH_2Cl_2 were collected fresh from an mBraun SPS-800 solvent purification system having been passed through anhydrous alumina columns. THF-d_8 was purchased from Fluorochem and degassed using freeze-thaw cycles and kept under argon over 3Å molecular sieves. Other deuterated solvents were purchased from Sigma-Aldrich. Unless stated otherwise, commercially available reagents were purchased from Sigma-Aldrich, Fisher Scientific, Apollo Scientific, Acros Organics, Strem Chemicals, Alfa Aesar or TCI UK and were used without purification. $[Rh(cod)(OH)]_2$ was purchased from Sigma Aldrich.

Analytical thin-layer chromatography was performed on pre-coated glass-backed plates (Silica Gel 60 F254; Merck) and visualised using a combination of UV light (254 nm) and aqueous ceric ammonium molybdate, aqueous basic potassium permanganate stains or *p*-anisaldehyde solution. Flash column chromatography was carried out using Apollo Scientific silica gel 60 (0.040 – 0.063 nm), Merck 60 Å silica gel, VWR (40-63 μm) silica gel and Sigma Aldrich silica gel. Pressure was applied at the column head *via* a flow of nitrogen. Heating was performed using Drysyn® heating blocks and the heating plate of the stirrer or using a Julabo FT902 immersion cooler.

Unless stated otherwise, solution NMR spectra were recorded at room temperature; ^{1}H, ^{2}H, ^{13}C, ^{31}P, ^{11}B, ^{19}F NMR and 2D NMR experiments were carried out using Bruker AVIII HD 400 (400/100 MHz), AVIII HD 500 (500/125 MHz) or AVII 500 (500/125 MHz) spectrometers. Chemical shifts are reported in ppm from the residual solvent peak. Chemical shifts (δ) are given in ppm and coupling constants (*J*) are quoted in hertz (Hz). Assignments were made with the assistance of gCOSY, gHSQC, gHMBC or NOESY NMR spectra.

Chiral HPLC separations were achieved using an Agilent 1230 Infinity series normal phase HPLC unit and HP Chemstation software. Chiralpak® columns (250 × 4.6 mm), fitted with matching Chiralpak® Guard Cartridges (10 × 4 mm), were used as specified in the text. Solvents used were of HPLC grade (Fisher Scientific, Sigma Alrich or Rathburn); all eluent systems were isocratic. Chiral SFC separations were conducted on a Waters Acquity UPC2 (Ultra Performance Convergence Chromatography) system equipped with a fluid delivery module (a liquid CO_2 pump and a modifier pump), a sampler manager (FL autosampler), a heated column manager 30s fitting eight

installed columns and a photodiode array detector. Daicel Chiralpak® IA-3, IB-3, IC-3, ID-3, IE-3, IF-3 or IG-3 columns were used as indicated.

Low resolution (LRMS) and high resolution (HRMS) mass spectral analyses were acquired by electrospray ionisation (ESI), electron impact (EI) and/or field ionisation (FI). Low resolution ESI were recorded using an Agilent 6120 quadrupole LC/MS. High resolution accurate ESI were recorded using a Thermo Exactive 1.1 SP5 Benchtop orbitrap MS and EI/FI on a Waters GTC Temperature programmed solid probe inlet within the department of chemistry, University of Oxford. Infrared measurements were carried out using a Bruker Tensor 27 FT-IR with internal calibration in the range 600-4000 cm^{-1}. Optical rotations were recorded on a Schmidt Haensch Unipol L2000 Polarimeter at 20 °C in a 10 cm cell in the stated solvent; [α]D values are given in 10^{-1} $deg.cm^2$ g^{-1} (concentration c given as g/100 mL).

Computational Methods

All density functional theory (DFT) calculations were performed with the Gaussian 09 program1 using the ωB97X-D functional. The split-valence 6-31G(d) basis set was used for C, N, O, H, P and Cl atoms, and LANL2DZ(f)3 (orbital exponent of 1.35) effective core potential/valence double zeta basis set with f polarisation function for Rh in all geometry optimisations. Single point energy corrections were obtained at the ωB97X-D /6-311+G(d,p) level of theory for C, N, O, H, P and Cl atoms, and ωB97X-D/LANL2TZ(f)4 effective core potential/valence triple zeta basis set with f polarisation function for Rh with an implicit description of the reaction medium (THF) by SMD solvent model as implemented in Gaussian09.

Gibbs free energies were evaluated at 333 K (the reaction temperature), for which the vibrational entropy contributions were computed using a free-rotor approximation for low frequency modes. A cut off frequency of 100 cm^{-1} was used as we switch between the rigid-rotor harmonic oscillator approximation for vibrations above this value and the free-rotor approximation below. For all mechanistic studies, a conventional standard state of 1 mol/L in solution for all species was employed. Harmonic vibrational frequencies were computed for all stationary points to confirm them as either minima or transition structures, possessing zero or a single imaginary frequency, respectively. All energetic terms were reported in kcal/mol. Molecular structures were visualised within the PyMOL Molecular Graphics System, Version 1.8 Schrödinger, LLC.

Data Availability Statement

Detailed experimental methods and analytical data for all experiments, along with absolute energies and selected distances for DFT computed structures for computed stationary points can be found in the supplementary information.

Code Availability Statement

All Python scripts used for data analysis have been made available - https://github.com/bobbypaton - under a creative commons CC-BY license.

References

(1) Hall, D.G. *Boronic Acids: Preparation and Applications in Organic Synthesis and Medicine*, Wiley-VCH, Weinheim, (2006).

(2) Suzuki, A. Cross-Coupling Reactions of Organoboranes: An Easy Way To Construct C-C Bonds (Nobel Lecture). *Angew. Chem. Int. Ed.* **50**, 6722–6737 (2011).

(3) Cherney, A.H., Kadunce, N.T. & Reisman, S.E. Enantioselective and Enantiospecific Transition-Metal-Catalyzed Cross-Coupling Reactions of Organometallic Reagents to Construct C-C Bonds. *Chem. Rev.* **115**, 9587–9652 (2015).

(4) Dong, L. et al. Asymmetric Nitroallylation of Arylboronic Acids with Nitroallyl Acetates Catalyzed by Chiral Rhodium Complexes and Its Application in a Concise Total Synthesis of Optically Pure (+)-γ-Lycorane. *Org. Lett.*, **7**, 4285–4288 (2005).

(5) Yu, B., Menard, F., Isono, N. & Lautens, M. Synthesis of Homoallylic Alcohols via Lewis Acid Assisted Enantioselective Desymmetrization. *Synthesis (Stuttg).* 853–859 (2009).

(6) Shintani, R., Takatsu, K., Takeda, M. & Hayashi, T. Copper-Catalyzed Asymmetric Allylic Substitution of Allyl Phosphates with Aryl- and Alkenylboronates. *Angew. Chem. Int. Ed*. **50**, 8656–8659 (2011).

(7) Zhang, P., Brozek, L.A. & Morken, J.P. Pd-Catalyzed Enantioselective Allyl-Allyl Cross-Coupling. *J. Am. Chem. Soc.* **132***,* 10686–10688 (2010).

(8) Chung, K., Miyake, Y. & Uemura, S. Nickel(0)-Catalyzed Asymmetric Cross-Coupling Reactions of Allylic Compounds with Grignard Reagents Using Optically Active Oxazolinylferrocenylphosphines as Ligands. *J. Chem. Soc*., *Perkin Trans. 1*, 2725–2729 (2000).

(9) Ohmiya, H., Makida, Y., Tanaka, T. & Sawamura, M. Palladium-Catalyzed γ-Selective and Stereospecific Allyl−Aryl Coupling between Allylic Acetates and Arylboronic Acids. *J. Am. Chem. Soc.* **130**, 17276–17277 (2008).

(10) Ohmiya, H., Yokokawa, N. & Sawamura, M. Copper-Catalyzed Gamma-Selective and Stereospecific Allyl-Aryl Coupling between (Z)-Acyclic and Cyclic Allylic Phosphates and Arylboronates. *Org. Lett.* **12**, 2438–2440 (2010).

(11) Sidera, M. & Fletcher, S.P. Rhodium-Catalyzed Asymmetric Allylic Arylation of Racemic Halides with Arylboronic Acids. *Nat. Chem.* **7**, 935–939 (2015).

(12) Schäfer, P., Palacin, T., Sidera, M. & Fletcher, S.P. Asymmetric Suzuki-Miyaura Coupling of Heterocycles via Rhodium-Catalyzed Allylic Arylation of Racemates. *Nat. Commun.* **8**, 15762–15769 (2017).

(13) González, J., van Dijk, L., Goetzke, F.W. & Fletcher, S.P. Highly enantioselective Rhodium-Catalyzed Cross-Coupling of Boronic Acids and Racemic Allyl Halides. *Nat Protoc*, **14,** 2972–2985 (2019).

(14) Goetzke, F.W., Mortimore, M. & Fletcher, S.P. Enantio- and Diastereoselective Suzuki‐Miyaura Coupling with Racemic Bicycles. *Angew. Chem. Int. Ed.* **58**, 12128–12132, **2019**.

(15) Hayashi, T., Takahashi, M., Takaya, Y. & Ogasawara, M. Catalytic Cycle of Rhodium-Catalyzed Asymmetric 1, 4-Addition of Organoboronic Acids. Arylrhodium, Oxa-π-Allylrhodium, and Hydroxorhodium Intermediates. *J. Am. Chem. Soc.* **124**, 5052–5058 (2002).

(16) Kina, A., Iwamura, H. & Hayashi, T. A Kinetic Study on Rh/Binap-Catalyzed 1,4-Addition of Phenylboronic Acid to Enones: Negative Nonlinear Effect Caused by Predominant Homochiral Dimer Contribution. *J. Am. Chem. Soc.* **128**, 3904–3905 (2006).

(17) Pfaltz, A., Lautens, M., Jacobsen, E.N., Pfaltz, A. & Yamamoto, H. *Comprehensive Asymmetric Catalysis II* (1999).

(18) Turnbull, B.W.H. & Evans, P.A. Asymmetric Rhodium-Catalyzed Allylic Substitution Reactions: Discovery, Development and Applications to Target-Directed Synthesis. *J. Org. Chem.* **83**, 11463–11479 (2018).

(19) You, H., Rideau, E., Sidera, M. & Fletcher, S.P. Non-Stabilized Nucleophiles in Cu-Catalyzed Dynamic Kinetic Asymmetric Allylic Alkylation. *Nature* **517**, 351–355 (2015).

(20) Rideau, E., You, H., Sidera, M., Claridge, T.D.W. & Fletcher, S.P. Mechanistic Studies on a Cu-Catalyzed Asymmetric Allylic Alkylation with Cyclic Racemic Starting Materials. *J. Am. Chem. Soc.* **139**, 5614–5624 (2017).

(21) Tsui, G. C., Menard, F. & Lautens, M. Regioselective Rhodium(I)-Catalyzed Hydroarylation of Protected Allylic Amines with Arylboronic Acids. *Org. Lett.* **12**, 2456–2459 (2010).

(22) Yang, Q., Wang, Y., Luo, S. & Wang, J. Kinetic Resolution and Dynamic Kinetic Resolution of Chromene by Rhodium-Catalyzed Asymmetric Hydroarylation. *Angew. Chem. Int. Ed*. **58**, 5343 –5347 (2019).

(23) Yang, X. et al. Catalytic Hydrothiolation: Counterion-Controlled Regioselectivity. *J. Am. Chem. Soc.* **141**, 3006−3013 (2019).

(24) Lu, Z., Wilsily, A. & Fu, G.C. Stereoconvergent Amine-Directed Alkyl-Alkyl Suzuki Reactions of Unactivated Secondary Alkyl Chlorides. *J. Am. Chem. Soc.* **133**, 8154–8157 (2011).

(25) Gutierrez, O., Tellis, J.C., Primer, D.N., Molander, G.A. & Kozlowski, M.C. Nickel-Catalyzed Cross-Coupling of Photoredox-Generated Radicals: Uncovering a General Manifold for Stereoconvergence in NickelCatalyzed Cross-Couplings. *J. Am. Chem. Soc.* **137**, 4896−4899 (2015).

(26) Langlois, J., Emery, D., Mareda, J. & Alexakis, A. Mechanistic identification and improvement of a direct enantioconvergent transformation in copper-catalyzed asymmetric allylic alkylation. *Chem. Sci.*, **3**, 1062−1069 (2012).

(27) Girard, C. & Kagan, H.B. Nonlinear Effects in Asymmetric Synthesis and Stereoselective Reactions: Ten Years of Investigation. *Angew. Chem. Int. Ed.* **37**, 2922–2959 (1998).

(28) Mc Daniel, D.H. & Brown, H.C. An Extended Table of Hammett Substituent Constants Based on the Ionization of Substituted Benzoic Acids. *J. Org. Chem.* **23**, 420–427 (1958).

(29) Corrie, T.J.A., Ball, L.T., Russell, C.A. & Lloyd-Jones, G. C. Au-Catalyzed Biaryl Coupling to Generate 5- to 9-Membered Rings: Turnover-Limiting Reductive Elimination versus π-Complexation. *J. Am. Chem. Soc.* **139**, 245–254 (2017).

(30) Lennox, A.J.J. & Lloyd-Jones, G.C. Transmetalation in the Suzuki–Miyaura Coupling: The Fork in the Trail. *Angew. Chem. Int. Ed.* **52**, 7362–7370 (2013).

(31) Thomas, A.A. & Denmark, S.E. Pre-transmetalation intermediates in the Suzuki-Miyaura reaction revealed: The missing link. *Science* **352**, 329–332 (2016).

(32) Yaman, T. & Harvey, J.N. Suzuki–Miyaura coupling revisited: an integrated computational study. *Faraday Discuss.* **220**, 425-442 (2019).

(33) Singleton, D.A. & Thomas, A.A. High-Precision Simultaneous Determination of Multiple Small Kinetic Isotope Effects at Natural Abundance. *J. Am. Chem. Soc.* **117**, 9357–9358 (1995).

(34) Frantz, D.E., Singleton, D.A. & Snyder, J. P. ^{13}C Kinetic Isotope Effects for the Addition of Lithium Dibutylcuprate to Cyclohexenone. Reductive Elimination Is Rate-Determining. *J. Am. Chem. Soc.* **119**, 3383–3384 (1997).

(35) Li, J. et al. Catalytic Asymmetric Cascade Vinylogous Mukaiyama 1,6-Michael/Michael Addition of 2-Silyloxyfurans with Azoalkenes: Direct Approach to Fused Butyrolactones. *J. Am. Chem. Soc.* **137**, 10124–10127 (2015).

(36) Colletto, C., Islam, S., Juliá-Hernández, F. & Larrosa, I. Room-Temperature Direct β-Arylation of Thiophenes and Benzo[*b*]Thiophenes and Kinetic Evidence for a Heck-Type Pathway. *J. Am. Chem. Soc.* **138**, 1677–1683 (2016).

(37) Smith, J.R. et al. Enantioselective Rhodium(III)-Catalyzed Markovnikov Hydroboration of Unactivated Terminal Alkenes. *J. Am. Chem. Soc.* **139**, 9148–9151 (2017).

(38) Rathbun, C.M. & Johnson, J.B. Rhodium-Catalyzed Acylation with Quinolinyl Ketones: Carbon−Carbon Single Bond Activation as the Turnover-Limiting Step of Catalysis. *J. Am. Chem. Soc.* **133**, 2031–2033 (2011).

(39) Moore, J.L., Silvestri, A.P., de Alaniz, J.R., DiRocco, D.A. & Rovis, T. Mechanistic Investigation of the Enantioselective Intramolecular Stetter Reaction: Proton Transfer Is the First Irreversible Step. *Org. Lett.* **13**, 1742–1745 (2011).

(40) Lee, D.H., Kwon, K.H. & Yi, C.S. Selective Catalytic C-H Alkylation of Alkenes with Alcohols. *Science* **333**, 1613–1616 (2011).

(41) Meyer, M.P. *New Applications of Isotope Effects in the Determination of Organic Reaction Mechanisms*, Elsevier, (2012).

(42) Vo, L.K. & Singleton, D.A. Isotope Effects and the Nature of Stereo- and Regioselectivity in Hydroaminations of Vinylarenes Catalyzed by Palladium(II)−Diphosphine Complexes. *Org. Lett.* **6**, 2469–2472 (2004).

(43) Roytman, V.A., Karugu R.W., Hong, Y., Hirschi, J.S. & Vetticatt, M.J. ^{13}C Kinetic Isotope Effects as a Quantitative Probe To Distinguish between Enol and Enamine Mechanisms in Aminocatalysis. *Chem. Eur. J.* **24**, 8098 –8102 (2018).

(44) Wolfsberg, M., Van Hook, W.A., Paneth, P. & Rebelo, L.P.N. Isotope Effects in the Chemical, Geological, and Bio Sciences; Springer, Dordrecht, (2010).

(45) Simmons, E.M. & Hartwig, J.F. On the Interpretation of Deuterium Kinetic Isotope Effects in C-H Bond Functionalizations by Transition-Metal Complexes. *Angew. Chem. Int. Ed.* **51**, 3066–3072 (2012).

(46) Deb, A., Hazra, A., Peng, Q. & Paton, R.S. Maiti, D. Detailed Mechanistic Studies on Palladium-Catalyzed Selective C−H Olefination with Aliphatic Alkenes - A Significant Influence of Proton Shuttling. *J. Am. Chem. Soc.* **139**, 763–775 (2017).

(47) Mekareeya, A. et al. Mechanistic insight into palladium-catalyzed cycloisomerization: A combined experimental and theoretical study. *J. Am. Chem. Soc.* **139**, 10104–10114 (2017).

(48) M. J. Frisch, et al, *Gaussian 09, Revision D.01*, Gaussian, Inc., Wallingford CT, (2009).

(49) Straker, R., Peng, Q., Mekareeya, A., Paton, R.S. & Anderson, E.A. Computational Ligand Design in Enantio- and Diastereoselective Ynamide [5+2] Cycloisomerizations. *Nature Commun.* **7**, 10109–10118 (2015).

(50) Peng, Q., Duarte, F. & Paton, R.S. Computing Organic Stereoselectivity – from Concepts to Quantitative Calculations and Predictions. *Chem. Soc. Rev.* **45**, 6093–6107 (2016).

(51) Karabiyikoglu, S., Brethomé, A., Palacin, T., Paton, R.S. & Fletcher, S.P. Enantiomerically enriched tetrahydropyridine allyl chlorides. *Chem. Sci.,* **11***,* 4125-4130 (2020).

(52) Mackenzie, P.B., Whelan, J. & Bosnich, B. Asymmetric synthesis. Mechanism of asymmetric catalytic allylation. *J. Am. Chem. Soc.* **107**, 2046-2054 (1985).

(53) Lloyd-Jones, G.C. & Stephen, S.C. Memory Effects in Pd-Catalysed Allylic Alkylation: Stereochemical Labelling through Isotopic Desymmetrization. *Chem. Eur. J.* **4**, 2539-2549 (1998).

(54) Lloyd-Jones, G.C. et al. Conclusive Evidence for a Retention−Retention Pathway for the Molybdenum-Catalyzed Asymmetric Alkylation. *J. Am. Chem. Soc.* **126**, 702-703 (2004).

(55) Madrahimov, S.T. & Hartwig, J.F. Origins of Enantioselectivity during Allylic Substitution Reactions Catalyzed by Metallacyclic Iridium Complexes *J. Am. Chem. Soc.* **134**, 8136–8147 (2012).

(56) Granberg, K.L. & Bäckvall, J.E. Isomerization of (π-Allyl)palladium Complexes *via* Nucleophilic Displacement by Palladium(0). A Common Mechanism in Palladium(0)-Catalyzed Allylic Substitution. *J. Am. Chem. Soc.* **114**, 6858–6863 (1992).

(57) Falivene, L. et al. Towards the Online Computer-Aided Design of Catalytic Pockets. *Nat. Chem.* **11,** 872–879 (2019).

Acknowledgments

The EPSRC supports this work though standard grant EP/N022246/1. L.v.D. and R.A. are grateful to the EPSRC Centre for Doctoral Training (CDT) in Synthesis for Biology and Medicine (EP/L015838/1) for studentships, generously supported by AstraZeneca, Diamond Light Source, Defence Science and Technology Laboratory, Evotec, GlaxoSmithKline, Janssen, Novartis, Pfizer, Syngenta, Takeda, UCB and Vertex. R.A. also acknowledges the Development and Promotion of Science and Technology Talents Project and the Royal Thai Government. This material is based upon work supported by the National Science Foundation under Grant No. 1955876. We used the Dirac cluster at Oxford supported by the EPSRC CDT for Theory and Modelling in Chemical Sciences (EP/L015722/1), the RMACC Summit supercomputer, which is supported by the National Science Foundation (ACI-1532235 and ACI-1532236), the University of Colorado Boulder and Colorado State University, and the Extreme Science and Engineering Discovery Environment (XSEDE) through allocation TG-CHE180056 and computing resources provided by the National e-Science Infrastructure Consortium, Thailand. O.S. thanks the Scientific and Technological Research Council of Turkey for the 2214-A Scholarship Programme. The research leading to these results has received funding from the European Research Council under the European Union's Seventh Framework Programme (FP7/2007-2013) / ERC grant agreement n° [838616].

Author Contributions

S.P.F. conceived and directed the project. S.P.F., L.v.D and M.S. designed the experiments. L.v.D., M.S. and S.K. performed the experiments. L.v.D., R.A., M.S., R.P., G.C.L.J. and S.P.F. analyzed the experimental results. R.S.P, L.v.D, R.A. and O.S. designed, conducted and analyzed the computational work. T.D.W.C. designed and performed the ^{13}C NMR experiments. G.C.L.J. derived the pseudo steady-state rate equation. L.v.D. and S.P.F. wrote the manuscript with contributions from R.S.P., G.C.L.J. T.D.W.C., M.S. and R.A..

Competing Interests

The authors declare no competing interests.